# Curvelet Based Texture Features for Breast Cancer Classifications

# Curvelet Based Texture Features for Breast Cancer Classifications

**Siti Salmah Yasiran, Shaharuddin Salleh, Norhaniza Sarmin, Rozi Mahmud, Suhaila Abd Halim.**

Center for Industrial and Applied Mathematics, Faculty of Sciences, Universiti Teknologi Malaysia, Johor Bahru, Johor. Malaysia

sitisalmah@tmsk.uitm.edu.my

**Abstract**. One of the sources of death among women is breast cancer. It is well known that Mammogram is the best method for breast cancer detection. Subsequently, there are solid requirements for the improvement of computer aided diagnosis (CAD) systems to assist radiologists in making decision. In this paper, the curvelet changes is proposed to classify the breast cancer. Curvelet refers to multi-level change which have the characteristics of directionality and anisotropy. It splits several characteristic impediments of wavelet to edges of an image. Two component extraction techniques were created associated with curvelet and wavelet coefficients to separate among various classes of breast. Finally, the K-Nearest Neighbor (KNN) classifiers were utilized to decide if the district is unusual or ordinary. The adequacy of the suggested strategies has been implemented with Mammographic Image Analysis Society (MIAS) data images. All the dataset is utilized by the suggested strategies. Then calculations have been applied with both curvelet and wavelet for correlation test were performed. The general outcomes show that curvelet change shows superior compared to the wavelet and the thing that matters is measurably noteworthy.

## 1. Introduction

Breast cancer disease is one of the significant concern's deaths around the world. As indicated by distributed insights of World Health Organization (WHO) approximate 460,000 deaths in 2010 [1]. Breast cancer is the main source of cancer in Malaysia. At any rate one in each 19 women in Malaysia is in danger of having breast cancer in the course of her life [1]. Early identification and therapy are viewed as the most encouraging ways to deal with diminish breast cancer death, since the reasons for the sickness are as yet obscure [2] . At the point when breast cancer is distinguished and treated early, the odds for recuperation are high. The current strategies for early identification of breast cancer are clinical breast tests and mammography. It can show changes of the breast as long as two years before a patient or doctor can detect the changes [3]. Mammographic irregularities which implies breast cancer can be classify into four types which are: microcalcifications, masses, design twisting and asymmetry.

Computer-Aided Diagnosis (CAD) systems is built to help radiologists in identifying mammographic sores that may show the existence of breast cancer. The CAD demonstration just as a subsequent and an ultimate conclusion is made by the radiologist. Computer aided design systems examine digitized or computerized mammography images utilizing programming projects to discover

features that related with breast cancer [4]. A Computer Aided Diagnosis (CADx) component have been proposed by Salleh et al., for breast cancer classifications. They have utilized the Speed Up Robust Features (SURF) method as their feature's extraction. The Principal Component Analysis (PCA) is also utilized to reduce the dimension of the feature's vectors. Three different classifiers are used to classify the cancer [5]. Recently, they have extended their finding with proposed Standard Deviation Based Otsu and also mathematical morphology as their features extraction [6-7].

Liu et al. [8] deteriorated the image utilizing multiresolution wavelet decay and at every goal level, separated a lot of features, including an edge direction histogram. Along these lines, every pixel was ordered by utilizing a paired choice tree. Sakellaropoulos et al. [9] utilized wavelet examination and feature extraction to characterize the pixels of the thick area as mass or typical tissue. At long last, there is an enormous arrangement of approaches dependent on Artificial Neural Netprocess (ANN) classifiers. These normally figured the issue of segmentation as a characterization of Region of Interest (ROI) as dubious or not. The features for preparing are power or surface related data dependent on a lot of realized ROI containing masses and a lot of arbitrary samples from typical tissue [10]. Christoyianni et al. [11] utilized a spiral based capacity neural system to order includes got from the histograms of every ROI. Hassanien et al. [12] and Ali and Hassanien [13] tried a heartbeat coupled neural system (PCNN), which can remove edges, image sections, and surface data from images. Mousa et al. [14] proposed a system dependent on wavelets investigation. They utilized a versatile neuro-fluffy deduction system (ANFIS) for building the classifier to recognize ordinary from anomalous.

### *1.1. Wavelet Tansform*

Jean Morlet have originally proposed the wavelet transform and created a novel mathematical tool for seismic wave analysis [15].The mother wavelet $\ell_{p,q}(r)$ defined as:

$$\ell_{p,q}(r) = \frac{1}{\sqrt{|q|}} \frac{(r-p)}{q}, \quad \text{where } p,q \in R,\ \mathrm{p} \neq 0 \tag{1}$$

The parameter $p$ refers to the scaling parameter, which measures the degree of compression. The parameter $q$ is the translation parameter. It is to control the time location of the wavelet. If $|q|<1$, this implies that the wavelet in Equation (1) is compressed wavelet to greater frequencies. If the value of $|p|>1$, then $\ell_{p,q}(r)$ has a larger time-width than $\ell(r)$ and corresponds to lower frequencies. Therefore, wavelets have the capability of time-widths obtained corresponding to their frequencies [15].

### *1.2. One-Dimensional Wavelet Transform*

The wavelet decomposition is an increasing sequence of closed subspaces $\{V_k\}k \in Z$ that approximate $M^2(R)$, where $Z$ and $R$ denote the sets of integers and real numbers, respectively. The terms $M^2(R)$ denotes the vector space of measurable square-integrable one-dimensional functions $f(x)$ [15]. The term $\varpi(t)$ refers to the scaling function. It can be expressed as;

$$\varpi_{2k}(t) = 2^k \varpi\left(2^k t\right) \tag{2}$$

then

$$(2^{-k})^{1/2} \varpi_{2k}\left(x - 2^{-k} m\right)_{(m,k)\in Z^2} \tag{3}$$

Equation (3) refers to an orthonormal basis obtained from dilation of a function with a coefficient $2^k$ and translation of the resulting function on a grid whose interval is proportional to $2^{-k}$. For any $m \in Z$

the scaling function is a member of $C_{2^k}$ that is included in $C_{2^{k+1}}$ $\left(C_{2^k} \subset C_{2^{k+1}}\right)$.The wavelet orthonormal basis is a family of functions that obtained thru the dilation and translation of the function $\ell(r)$. The wavelet representation is the orthogonal complement of the original signal space, $V_{2^k}$. Denote the complement space as $O_{2^k}$. Let

$$\ell_{2^k}(r) = 2^k \ell\left(2^k r\right) \tag{4}$$

represents the dilation of $\ell(y)$ by $2^k$.

$$(2^{-k})^{1/2} \ell_{2^k}\left(x - 2^{-k} m\right)_{(m,k)\in Z^2} \tag{5}$$

is an orthonormal basis that can be computed by scaling the wavelet with a coefficient $2^k$ and translating it on a grid with the corresponding interval is proportional to $2^{-k}$. The difference between signal at resolutions $2^{k+1}$ and $2^k$ can be extracted on a wavelet orthonormal basis of $M^2(R)$. The decomposition become a new signal approximation and a detail signal. The signal approximation is given by

$$\hat{f}_{2^k}(x) = \sum_i \left\{ \left\langle \varpi_{2^{-1}}(x), \varpi\left[x - (i - 2m)\right] \right\rangle \times \left\langle f(x), \varpi_{2^{k+1}}\left(x - 2^{-k-1} i\right) \right\rangle \right\}, \tag{6}$$

where $i \in Z$ and $\langle a,b \rangle$ is the inner product of $a$ and $b$. The resolution change is obtained by the first inner product, which acts as a low-pass filter,

$$\Upsilon(m) = \left\langle \varpi_{2^{-1}}(x), \varpi(x - m) \right\rangle \tag{7}$$

and by subsampling by two with use of Equation (6), Equation (7), the signal will become

$$\hat{f}_{2^k}(x) = \sum_i \tilde{h}(2x - i)\, \hat{f}_{2^{k+1}}(i), \tag{8}$$

where we assume that $\tilde{\Upsilon}(m) = \Upsilon(-m)$.

*1.3. Two-Dimensional Wavelet Transform*

It is already well known that, the extended version of the one-dimensional is called the two-dimensional wavelet. It can be interpreted as a one-dimensional wavelet transform along the $x$and $y$ axes. As in the one-dimensional case, the original image is reduced in resolution by a low-pass filter and subsampling to form an approximation image, but this time it is for both rows and columns of the image. This is a separable multiresolution approximation of $M^2(R^2)$ in which the scaling function is

$$\Phi(x,y) = \Phi(x)\Phi(y) \tag{9}$$

The resulting two-dimensional decomposition at a given resolution level also results in detail images that are threefold. The three detail images are a set of independent, spatially oriented frequency channels that detail vertical high frequencies, horizontal high frequencies, and cross-directional high frequencies. The three wavelets that give these detail images are

$$\Psi^1(x,y)=\phi(x)\psi(y),$$
$$\Psi^2(x,y)=\phi(x)\psi(y), and \quad (10)$$
$$\Psi^3(x,y)=\phi(x)\psi(y).$$

The wavelet model can be reached into two-dimensional signs by divisible multiresolution value scaling capacity in Equation (8). There are three related wavelet capacities from Equation (10), represent the wavelet deterioration of a two-dimensional sign can be registered with a detachable expansion of the one-dimensional decay calculation.

## 2. Proposed Method

Figure 2.1 represents the means of the proposed computer aided diagnosis system.

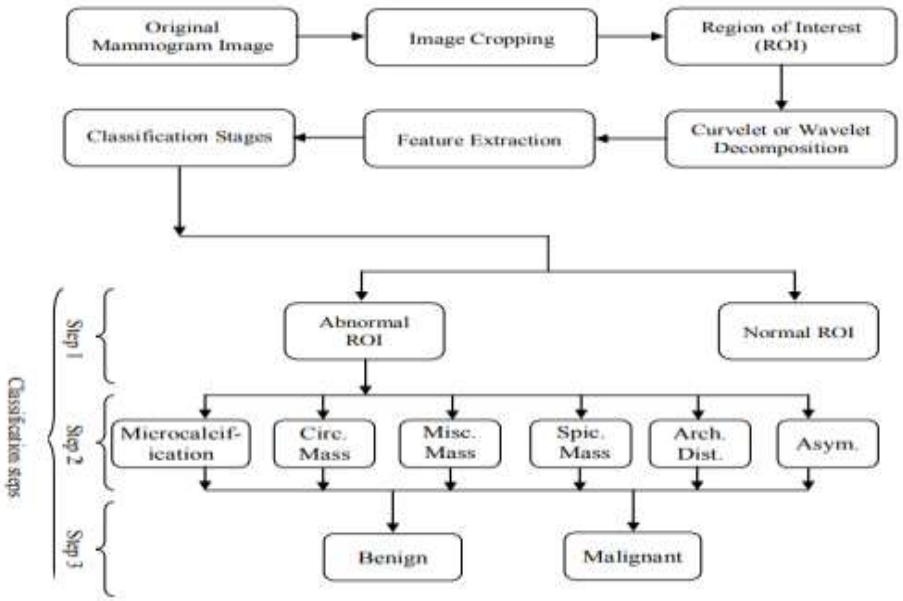


**Figure 2.1**: The proposed computer aided diagnosis system.

From Figure 2.1, the first part contains the advancement of a computer aided diagnosis system. In this part, the ROI are removed physically. The multiresolution portrayals curvelet and wavelet are then used to disintegrate the ROIs. Subsequently, two component extraction techniques are introduced to recognize the various classes of breast cancer. The first techniques are features extraction based on a percentage of biggest coefficients. This is followed by features extraction curvelet based texture feature extraction. Both methods will be discussed in the next section.

In the second part, ROIs are recognized consequently implemented by curvelet disintegration and feature extraction strategies from part 1. In this paper, the classification steps include all the three steps as illustrates in Figure 2. Firstly, the classification is focus on to classify either it is abnormal or normal ROI. This is followed by the classification of six types abnormalities of the ROI. The abnormalities include microcalcifications, circumscribed masses, misclassification masses, speculated masses, architectural distortion and asymmetric, Finally, the classification is focus to classify either is the abnormal ROI is benign or malignant. All of these classification rates are determined by utilizing KNN.

### *2.1. Feature Extraction Based of the Biggest Coefficients Value*

In order to decay the ROIs into four disintegration levels, both curvelets and wavelets are implemented. Various proportions from the greatest coefficients from every decay level are utilized as the element vectors. Then, the ratio of coefficient for both class vector and mammogram will be embedded into KNN classifier. The strategy of the element extraction and characterization technique illustrates in Figure 3.

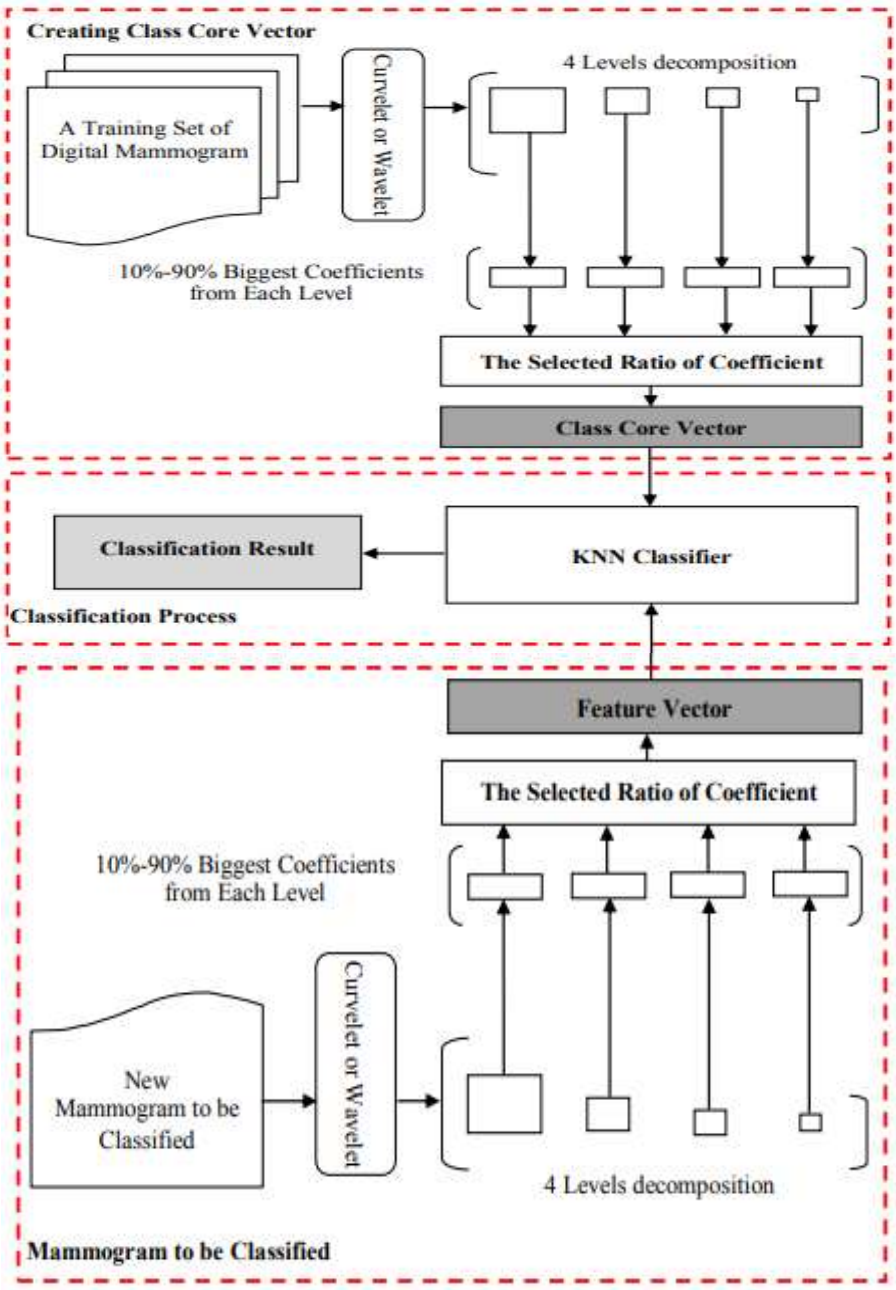


**Figure 2.2**: The proposed features by extracting ratio of the biggest coefficient value.

From Figure 2.2, the proportions are taken in the range of 10% and 90% of coefficients from each level. Then, it will be gathered in one vector to be embedded to the KNN classifier to be classified. This study utilized the 70% of training dataset and 30% testing rules.

*2.2. Feature Extraction Curvelet Based Texture Feature Extraction Method*

After the ROI have been trimmed, the curvelet change is applied on ROI. At that point, seven measurable properties for each wedge are determined. The properties are: Energy, Entropy, Mean, Standard Deviation, Maximum Probability, Inverse Difference Moment and Homogeneity. These properties are portrayed in Figure 2.3.

$$\text{Energy} = \sum_i^M \sum_j^N I^2[i,j]$$

$$\text{Entropy} = -\sum_i^M \sum_j^N I[i,j]\ log\ I[i,j]$$

$$\text{Mean} = \frac{1}{M*N} \sum_i^M \sum_j^N I[i,j]$$

$$\text{STD} = \sqrt{(I[i,j] - \bar{I}[i,j])^2}$$

$$\text{Max Probability} = \max I[i,j]$$

$$\text{Inverse Difference Moment} = \sum_i^M \sum_j^N \frac{I[i,j]}{|i-j|^2}\ where\ i \neq j$$

$$\text{Homogeneity} = \sum_i^M \sum_j^N \frac{I[i,j]}{1+(i+j)^2}$$

**Figure 2.3**: The seven texture features extracted from each wedge in curvelet decomposition

From Figure 2.3, the curvelet is utilized with scale four and sixteen points, then it is disintegrated into 81 slices. After that, the features are determined for each slice, with the goal of 567 features as the value of features vector. Table 2.1 illustrates the quantity of features obtained after applying the component extraction strategy.

**Table 2.1**: The number of features before and after execution of the strategy.

| Function | total features before feature extraction | total features after feature extraction |
|---|---|---|
| Normal vs. abnormal | 567 | 220 |
| Benign vs. malignant | 567 | 222 |

From Table 2.1, the most critical features are acquired by the feature's vectors to a standard deviation of average component extraction technique. It begins with computing a mean features vector for every class. Then, the standard deviation vector is determined. The rest of the features will be the features vector for the comparing ROI. The chose features then will be utilized to for various classes. The past created two strategies of extraction were implemented to ROIs and physically edited from the first steps.

## 3. Results and Discussion

The initial step is to trim the ROIs physically from the first mammogram. Also, two elements of features extraction strategies are utilized to recognize the most critical features. Therefore, the attained features are embedded to the classifiers. The consequences of this part are discussed as follows.

### *3.1. Results of Feature Extraction Based of the Biggest Coefficients Value*

The wavelet and curvelet are implemented to four levels. From every decay level, a proportion of the greatest coefficients then utilized to be the element vector of corresponding mammogram. Thus, every ROI will be initiated in four rates, every rate chose from various scale. It is chosen from 10% to 90%. Then, the vectors are embedded to KNN to classify into various classes. The acquired outcomes from KNN classifier to recognize irregular and typical classes are introduced in Table 3.1.

**Table 3.1**: Accuracy rates between abnormal and normal classes.

| Method | class | 10% | 20% | 30% | 40% | 50% | 60% | 70% | 80% | 90% |
|---|---|---|---|---|---|---|---|---|---|---|
| Curvelet | Abnormal | 97.50 | 95.95 | 98.01 | 96.41 | 98.46 | 97.35 | 97.11 | 97.35 | 93.97 |
| | Normal | 92.59 | 96.30 | 96.30 | 92.59 | 88.89 | 100.00 | 96.30 | 96.30 | 96.30 |
| | W. Average | 94.34 | 96.18 | 96.91 | 93.95 | 92.31 | 99.05 | 96.59 | 96.68 | 95.47 |
| Wavelet | Abnormal | 95.86 | 85.09 | 89.83 | 87.90 | 95.83 | 87.73 | 89.86 | 90.53 | 93.62 |
| | Normal | 77.78 | 100.00 | 100.00 | 96.30 | 88.89 | 100.00 | 88.89 | 100.00 | 77.78 |
| | W. Average | 84.24 | 94.68 | 96.37 | 93.30 | 91.37 | 95.62 | 89.24 | 96.62 | 83.44 |

From table 3.1, it shows that the most noteworthy normal arrangement precision rate acquired with curvelet coefficients was 99.05%. Meanwhile, it was 95.62% utilizing 60% of coefficients. It is clearly seen that curvelet perform higher average classification accuracy rates compared to the wavelet in each percentage ratio from the biggest coefficients. Table 3.2 presents the order accuracy rates accomplished in separating between the variations from the norm classes dependent on their shapes. For every rate, a normal of precision rate is determined and an examination is refined among curvelet and wavelet.

**Table 3.2**: Accuracy rate between different abnormalities.

| Method | Class | 10% | 20% | 30% | 40% | 50% | 60% | 70% | 80% | 90% |
|---|---|---|---|---|---|---|---|---|---|---|
| Curvelet | Calc | 96.00 | 92.00 | 100.00 | 100.00 | 96.00 | 96.00 | 96.00 | 96.00 | 92.00 |
| | Circ | 95.65 | 95.65 | 100 | 95.65 | 100.00 | 100.00 | 100.00 | 100.00 | 95.65 |
| | Ill-def | 100.00 | 100.00 | 100.00 | 100.00 | 100.00 | 100.00 | 100.00 | 100.00 | 100.00 |
| | Spic | 100.00 | 100.00 | 94.74 | 94.74 | 94.74 | 94.74 | 100.00 | 94.74 | 94.74 |
| | Arch | 100.00 | 94.74 | 100.00 | 94.74 | 100.00 | 100.00 | 100.00 | 100.00 | 94.74 |
| | Asym | 93.33 | 93.33 | 93.33 | 93.33 | 100.00 | 93.33 | 86.67 | 93.33 | 86.67 |
| | W. Average | 97.39 | 95.65 | 98.26 | 96.52 | 98.26 | 97.39 | 97.39 | 97.39 | 93.91 |
| Wavelet | Calc | 100.00 | 64.00 | 60.00 | 80.00 | 100.00 | 100.00 | 76.00 | 80.00 | 88.00 |
| | Circ | 100.00 | 95.65 | 100.00 | 100.00 | 95.65 | 86.96 | 100.00 | 100.00 | 100.00 |
| | Ill-def | 85.71 | 100.00 | 100.00 | 100.00 | 100.00 | 85.71 | 100.00 | 100.00 | 100.00 |
| | Spic | 89.47 | 84.21 | 84.21 | 84.21 | 52.63 | 100.00 | 73.68 | 100.00 | 94.74 |
| | Arch | 100.00 | 100.00 | 94.74 | 63.16 | 100.00 | 73.68 | 89.47 | 63.16 | 78.95 |
| | Asym | 100.00 | 66.67 | 100.00 | 100.00 | 126.67 | 80.00 | 100.00 | 100.00 | 100.00 |
| | W. Average | 96.52 | 84.35 | 87.83 | 86.96 | 94.78 | 88.70 | 88.69 | 89.57 | 93.04 |

From Table 3.2, it can be observed that the curvelet outflanks wavelet for each grouping abnormalities. The acquired outcomes by removing a level of the greatest coefficients from 4 scales deterioration of curvelet and wavelet indicate that few rates implies that the classifier accomplishes great accuracy.

The order precision rates accomplished to separate between the generous and threatening classes are introduced in Table 3.3.

**Table 3.3** Accuracy rates between benign and malignant.

| Method | class | 10% | 20% | 30% | 40% | 50% | 60% | 70% | 80% | 90% |
|---|---|---|---|---|---|---|---|---|---|---|
| Curvelet | Benign | 98.44 | 100.00 | 100.00 | 100.00 | 100.00 | 98.44 | 98.44 | 100.00 | 100.00 |
| | Malign | 100.00 | 100.00 | 90.20 | 100.00 | 98.04 | 100.00 | 100.00 | 100.00 | 100.00 |
| | W. Average | 99.13 | 100.00 | 95.65 | 100.00 | 99.13 | 99.13 | 99.13 | 100.00 | 100.00 |
| Wavelet | Benign | 51.56 | 100.00 | 98.44 | 85.94 | 93.75 | 100.00 | 68.75 | 100.00 | 89.06 |
| | Malign | 100.00 | 92.16 | 100.00 | 100.00 | 100.00 | 100.00 | 100.00 | 100.00 | 100.00 |
| | W. Average | 73.04 | 96.52 | 99.13 | 92.18 | 96.52 | 100.00 | 82.61 | 100.00 | 93.91 |

From Table 3.3, the normal of the capacity of every rate is determined and an examination is practiced among curvelet and wavelet at every rate. It can also be observed that curvelet outflanks wavelet in arranging mammogram images among generous and harmful cases.

### *3.2. Results of Features Extraction using Standard Deviation of Means*

Data is partitioned into two categories. For every category, it is composed of various images of all accessible classes. The main category is utilized to develop the component vectors, while the subsequent category is utilized to test the proposed strategy. Wavelet and curvelet changes are utilized to be implemented to the ROIs of mammogram images. Then it will extricate coefficients to be embedded to the classifier. Then, four deterioration levels are utilized. The mean of each class of images is finalized. At that point the standard deviation of the lattice of methods for lasses is determined to create a vector to the standard deviations section by segment. The hard edge value is determined according to [16], where X refers to length of the coefficients vector. Table 3.4 shows the quantity of coefficients with the limit.

**Table 3.4**: Coefficients of wavelet and curvelet foe three types of problems.

| Problem | Wavelet | | Curvelet | |
|---|---|---|---|---|
| | before threshold (N) | after threshold (L) | before threshold (N) | after threshold (L) |
| Normal vs. abnormal | 25129 | 722 | 46080 | 1619 |
| Abnormality types | 25129 | 2141 | 46080 | 2066 |
| Benign vs. malignant | 25129 | 1144 | 46080 | 1091 |

From Table 3.4, the proposed strategy is applied to cover the three mammogram characterization issues. The initial step is the order of ordinary versus irregular classes. The subsequent advance is the grouping of anomaly pointer dependent on their shape. The third step is to separate among generous and threatening tumours. In this process, the normal of grouping accuracy rates is determined dependent on 2x5-folds cross approval. The proposed strategy is focused with the technique for greatest 100 coefficients introduced earlier. Table 3.5 presents the characterization precision rates accomplished in separating among typical and strange classes.

**Table 3.5**: Accuracy rates using standard deviation for curvelet and wavelet.

| Method | Class | Partitions 1 | | | | | Partitions 2 | | | | | Average |
|---|---|---|---|---|---|---|---|---|---|---|---|---|
| | | Fold 1 | Fold 2 | Fold 3 | Fold 4 | Fold 5 | Fold 1 | Fold 2 | Fold 3 | Fold 4 | Fold 5 | |
| Curvelet | Abnormal | 100.00 | 100.00 | 100.00 | 100.00 | 100.00 | 100.00 | 100.00 | 100.00 | 100.00 | 100.00 | 100.00 |
| | Normal | 95.06 | 93.72 | 93.72 | 94.20 | 94.20 | 93.72 | 94.20 | 94.20 | 95.65 | 94.20 | 94.29 |
| | W. Average | 96.82 | 95.96 | 95.96 | 96.27 | 96.27 | 95.96 | 96.27 | 96.27 | 97.20 | 96.27 | 96.33 |
| Wavelet | Abnormal | 100.00 | 100.00 | 100.00 | 100.00 | 100.00 | 100.00 | 100.00 | 100.00 | 100.00 | 100.00 | 100.00 |
| | Normal | 91.30 | 90.82 | 91.79 | 91.3 | 91.79 | 91.79 | 92.75 | 91.79 | 91.30 | 90.82 | 91.55 |
| | W. Average | 94.41 | 94.10 | 94.72 | 94.41 | 94.72 | 94.72 | 95.34 | 94.72 | 94.41 | 94.10 | 94.57 |

From Table 3.5, it can be observed that all classification rate is above 90%. Two partition are applied with 5 folds for each partition which represents the 2x5-folds cross approval. It can be observed that both curvelet represent the highest accuracy compared to the wavelet. For standard deviation of means, there are slightly difference between both methods which is 1.57. Meanwhile for biggest 100 coefficient, the classifications accuracy rates of curvelet exceed the wavelet by 4.41. Table 3.6 presents the order accuracy paces of irregularity types as per their shapes.

**Table 3.6**: Accuracy rates for seven types of abnormalities classifications.

| Method | Class | Partitions 1 | | | | | Partitions 2 | | | | | Average |
|---|---|---|---|---|---|---|---|---|---|---|---|---|
| | | Fold 1 | Fold 2 | Fold 3 | Fold 4 | Fold 5 | Fold 1 | Fold 2 | Fold 3 | Fold 4 | Fold 5 | |
| Curvelet | Calc | 100.00 | 100.00 | 100.00 | 100.00 | 92.00 | 100.00 | 100.00 | 96.00 | 96.00 | 96.00 | 98.00 |
| | Circ | 91.30 | 91.30 | 91.30 | 86.96 | 86.96 | 95.65 | 95.65 | 95.65 | 95.65 | 91.30 | 92.17 |
| | Misc | 100.00 | 100.00 | 100.00 | 100.00 | 92.86 | 100.00 | 100.00 | 100.00 | 100.00 | 100.00 | 99.29 |
| | Spic | 100.00 | 100.00 | 94.74 | 100.00 | 100.00 | 94.74 | 94.74 | 94.74 | 94.74 | 94.74 | 96.84 |
| | Arch | 89.47 | 89.47 | 84.21 | 89.47 | 89.47 | 94.74 | 94.74 | 94.74 | 89.47 | 100.00 | 91.58 |
| | Asym | 100.00 | 100.00 | 100.00 | 100.00 | 100.00 | 100.00 | 100.00 | 100.00 | 100.00 | 100.00 | 100.00 |
| | W. Average | 96.52 | 96.52 | 94.78 | 95.65 | 93.04 | 97.39 | 97.39 | 96.52 | 95.65 | 96.52 | 96.00 |
| Wavelet | Calc | 92.00 | 96.00 | 100.00 | 92.00 | 100.00 | 96.00 | 100.00 | 100.00 | 96.00 | 96.00 | 96.80 |
| | Circ | 86.96 | 91.30 | 95.65 | 91.30 | 86.96 | 95.65 | 100.00 | 95.65 | 95.65 | 95.65 | 93.48 |
| | Misc | 92.86 | 92.86 | 100.00 | 92.86 | 100.00 | 100.00 | 100.00 | 85.71 | 100.00 | 100.00 | 96.43 |
| | Spic | 100.00 | 78.95 | 94.74 | 89.47 | 100.00 | 84.21 | 89.47 | 94.74 | 94.74 | 89.47 | 91.58 |
| | Arch | 94.74 | 100.00 | 89.47 | 84.21 | 94.74 | 78.95 | 100.00 | 89.47 | 94.74 | 100.00 | 92.63 |
| | Asym | 100.00 | 100.00 | 100.00 | 100.00 | 100.00 | 100.00 | 100.00 | 100.00 | 100.00 | 100.00 | 100.00 |
| | W. Average | 93.91 | 93.04 | 96.52 | 91.30 | 96.52 | 92.17 | 98.26 | 94.78 | 96.52 | 96.52 | 94.96 |

From Table 3.6, it can be observed that the arrangement of coefficients separated from curvelet change accomplishes higher grouping rate contrasted with wavelet coefficients. It shows also that the proposed strategy is superior compared to the technique for removing the greatest 100 coefficients from deterioration levels. Again, it can be observed that both curvelet represent the highest accuracy compared to the wavelet. For standard deviation of means, there are slightly difference between both methods which is 0.79. Meanwhile for biggest 100 coefficient, the classifications accuracy rates of curvelet exceed the wavelet by 6.28. Table 3.7 represent the classification accuracy rates between both methods to classify the cancer either it is benign or malignant.

**Table 3.7**: Accuracy rates obtained for bengin and malignant classifications.

| Method | Class | Partitions 1 | | | | | Partitions 2 | | | | | Average |
|---|---|---|---|---|---|---|---|---|---|---|---|---|
| | | Fold 1 | Fold 2 | Fold 3 | Fold 4 | Fold 5 | Fold 1 | Fold 2 | Fold 3 | Fold 4 | Fold 5 | |
| Curvelet | Benign | 95.31 | 93.75 | 95.31 | 92.19 | 93.75 | 95.31 | 92.19 | 95.31 | 89.06 | 92.19 | 93.44 |
| | Malignant | 100.00 | 100.00 | 100.00 | 100.00 | 100.00 | 100.00 | 100.00 | 100.00 | 100.00 | 100.00 | 100.00 |
| | W. Average | 97.39 | 96.52 | 97.39 | 95.65 | 96.52 | 97.39 | 95.65 | 97.39 | 93.91 | 95.65 | 96.35 |
| Wavelet | Benign | 93.75 | 92.19 | 95.31 | 90.63 | 90.63 | 93.75 | 90.63 | 95.31 | 87.50 | 90.63 | 92.03 |
| | Malignant | 100.00 | 100.00 | 100.00 | 100.00 | 100.00 | 100.00 | 100.00 | 100.00 | 100.00 | 100.00 | 100.00 |
| | W. Average | 96.52 | 95.65 | 97.39 | 94.79 | 94.79 | 96.52 | 94.79 | 97.39 | 93.04 | 94.79 | 95.56 |

From Table 3.7, based on the highlighted rows, it shows the threatening class has been characterized. Overall, curvelet still outflanks wavelet. This means that the proposed strategy gives grouping higher rates.

## 4. Conclusion and Recommendation

A curvelet changes-based CAD in mammogram proposed. This paper concentrated on develop the computer aided diagnosis system by creating two methods for features extraction. In this process, the KNN classifiers is utilized to separate between various classes. The general outcomes from this strategy show that curvelet beats wavelet.

There is some suggestion for future investigations and currently investigated:1) Reconstruction of separated coefficients of curvelet and wavelet may be reasonable to recognize the irregularity of first mammogram images.2) Integrating other imaging modalities, for sample, ultrasound, attractive reverberation imaging (MRI) and registered tomography (CT) with X-beam mammography.

**Acknowledgement**

The author(s) would like to thanks Persatuan Sains Matematik Malaysia (PERSAMA) for supporting this research.

## References

[1] Joy J E, Penhoet E E and Petitti D B 2005 Saving women's lives: strategies for improving breast cancer detection and diagnosis

[2] Rangayyan R M, Ayres F J and Leo Desautels J E 2007 A review of computer-aided diagnosis of breast cancer: Toward the detection of subtle signs *J. Franklin Inst.* **344** 312–48

[3] Bhosle M, Samuel S, Vosuri V, Paskett E and Balkrishnan R 2007 Physician and patient characteristics associated with outpatient breast cancer screening recommendations in the United States: Analysis of the National Ambulatory Medical Care Survey Data 1996-2004 *Breast Cancer Res. Treat.* **103** 53–9

[4] Helvie M 2007 Improving Mammographic Interpretation: Double Reading and Computer-Aided Diagnosis *Radiol. Clin. North Am.* **45** 801–11

[5] Salleh S, Mahmud R, Rahman H and Yasiran S S 2017 Speed up Robust Features (SURF) with Principal Component Analysis-Support Vector Machine (PCA-SVM) for benign and malignant classifications *J. Fundam. Appl. Sci.* **9** 624–43

[6] Yasiran S S, Salleh S and Mahmud R 2020 Standard Deviation Based Otsu for Breast Cancer Classification *ASM Sci. J.*

[7] Yasiran S S, Salleh S and Mahmud R 2020 Otsu and Mathematical Morphology for Breast Cancer Classification *ASM Sci. J.*

[8] Liu S, Babbs C F and Delp E J 2001 Multiresolution detection of spiculated lesions in digital mammograms *IEEE Trans. Image Process.* **10** 874–84

[9] Sakellaropoulos F, Skiadopoulos S, Karahaliou A, Costaridou L and Panayiotakis G 2006 Using wavelet-based features to identify masses in dense breast parenchyma *International Workshop on Digital Mammography* (Springer) pp 557–64
[10] Oliver A, Freixenet J, Marti J, Perez E, Pont J, Denton E R E and Zwiggelaar R 2010 A review of automatic mass detection and segmentation in mammographic images *Med. Image Anal.* **14** 87–110
[11] Christoyianni I, Dermatas E and Kokkinakis G 2000 Fast detection of masses in computer-aided mammography *IEEE Signal Process. Mag.* **17** 54–64
[12] Hassanien A E, Ali J M and Nobuhara H 2004 Detection of spiculated masses in Mammograms based on fuzzy image processing *International Conference on Artificial Intelligence and Soft Computing* (Springer) pp 1002–7
[13] Ali J M H and Hassanien A E 2006 PCNN for detection of masses in digital mammogram *Neural Netw. World* **16** 129
[14] Mousa R, Munib Q and Moussa A 2005 Breast cancer diagnosis system based on wavelet analysis and fuzzy-neural *Expert Syst. Appl.* **28** 713–23
[15] Yocky D A 1995 Image merging and data fusion by means of the discrete two-dimensional wavelet transform *J. Opt. Soc. Am. A* **12** 1834
[16] Donoho D L and Johnstone J M 1994 Ideal spatial adaptation by wavelet shrinkage *Biometrika* **81** 425–55